

# Fabrication of PVDF/PMMA Polymer for Sustainable Energy Harvesting

J.R. Leppe-Nerey<sup>1</sup>, F.Z. Sierra-Espinosa<sup>2,\*</sup>, M.E. Nicho<sup>2</sup>, M.A. Basurto<sup>2</sup> and J.A. Rodríguez<sup>2</sup>

<sup>1</sup>Posdoctorado en Ingeniería y Ciencias Aplicadas, Universidad Autónoma del Estado de Morelos, Av. Universidad 1001, Campus Chamilpa, 62209 Cuernavaca, Morelos, México

<sup>2</sup>Centro de Investigación en Ingeniería y Ciencias Aplicadas, Universidad Autónoma del Estado de Morelos, Av. Universidad 1001, Col. Chamilpa, C.P. 62209, Cuernavaca, Morelos, México

**Abstract:** The synthesis of blends that combine properties of two or more polymeric materials is increasingly investigated due to the versatility of the synthesis and its growing potential for many applications, including sustainability. Their characteristics are defined mainly by the synthesis conditions. Therefore, this paper details the synthesis process of easy-to-handle films using mixing method. The procedures and drawbacks found during the preparation of composite films are described. Polymeric compounds formed by the mixture of polyvinylidene fluoride (PVDF) and polymethyl methacrylate (PMMA) are addressed, varying the concentration, and evaluating their impact on the piezoelectric capacity. Films were formed through the spin-coating technique and characterized by optical and holographic microscopes. The results showed that composites with a concentration of 50 wt.% or larger of PVDF in the blend acquire a morphology with a granular appearance, however at lower concentrations they present a homogeneous morphology similar to that of PMMA. A homogeneous distribution of PVDF in the PMMA stands out. However, excessive contents of PMMA are associated to peaks and non-uniformities detected like multicolored regions by digital holography. Controlled strength-strain laboratory tests allowed to evaluate the film blends performance. The results indicate noticeable improvements in voltage output for a composition 70wt% PVDF and 30 wt% PMMA.

**Keywords:** Polymer blends, PVDF, PMMA, Power generation, Energy harvesting, Piezoelectricity, OM, DHM.

## 1. INTRODUCTION

The realization of mixtures and compounds that combine the properties of interest of two or more polymeric materials is increasingly studied in the world, to obtain a material that has the ideal characteristics for specific application. The interest in these materials is due to their versatility and potential broad use. A key challenge in energy harvesting is to obtain a competitive composition from raw materials. By developing blends of varied materials, the cost of the mixture can be up to ten times less than that of a branded film [1-3]. Thus, the possibility of improving the procedure used to develop new composites to reduce costs and increase performance remains open. For instance, considering nanocomposites through multiple or single carbon nanotubes.

Polyvinylidene fluoride (PVDF), a semicrystalline polymer, presents fascinating mechanical, pyroelectric, piezoelectric and film-forming properties making it of interest for scientific research, widely applied in various industries and their processes due to its superior properties [4]. Currently it is used to fabricate different

sensors, strain gauges, immunoblotting membranes, audio transducers, among other products [5-9]. This polymer has a simple chemical structure with five crystalline phases ( $\alpha$ ,  $\beta$ ,  $\gamma$ ,  $\delta$  and  $\epsilon$  phase) depending on the different processing methods used; its strong ferroelectric behavior is due to  $\beta$  phase. In this phase, the polymer chains are aligned so that their respective directions of polarization are the same, making it the most polar phase of PVDF [10]. However, commercially developed PVDF is mainly available as a single  $\alpha$ -phase, since in its pristine form, the  $\beta$ -phase is thermodynamically unstable [11-13]. In addition, their production costs are high, which demerits its competitiveness for profitable technological applications [1]. Therefore, to produce a novel material in addition to retain electrical properties being less expensive than existing, we blended PVDF with oxygen-containing polymers such as polymethyl methacrylate (PMMA) [1, 2, 13-15]. The miscibility of the two polymers is effective due to the presence of strong hydrogen group bonds between the carbonyl groups of PMMA and the  $\text{CH}_2$  groups of PVDF, and the effective dipole bonds between the  $\text{CH}_2$  groups of PMMA and the  $\text{CF}_2$  groups of PVDF [16-17]. Interestingly, we found PVDF crystallize in the  $\beta$ -phase when mixed with PMMA at a production cost significantly reduced [1]. Deeba *et al.* [10] reported on

\*Address correspondence to this author at Centro de Investigación en Ingeniería y Ciencias Aplicadas, Universidad Autónoma del Estado de Morelos, Av. Universidad 1001, Col. Chamilpa, C.P. 62209, Cuernavaca, Morelos, México; E-mail: fse@uaem.mx

the fabrication of polymeric films based on a blend of PMMA and PVDF prepared by the solution casting method, varying the wt.% ratio of the polymers. In addition, there are investigations in which other components are used for PVDF samples to improve chemical, mechanical and electrical properties, to increase chemical resistance, elasticity, mechanical strength, conductivity, electrical generated output, etc. Among these components, and their mixtures, are PMMA [18], Zirconia Titanate (PZT) [19], Barium titanate ( $\text{BaTiO}_3$ ) [20], cellulose [21], Single and Multiwalled Carbon Nanotubes (SWCNTs-MWCNTs) [20, 22-26], always looking for improving the PVDF polymeric matrix by converting  $\alpha$  phase into  $\beta$  phase. It is important to mention that none of these describe in detail the steps followed during preparation of samples, and even less for the preparation of films for use in a testing device.

A review of the literature showed that studies on PVDF/PMMA blends investigated optical, mechanical, and thermal behavior, for instance stretching that may improve transformation of  $\alpha$  into  $\beta$  phase in PVDF films [27-28]; however, there have been few systematic studies on electrical behavior [29]. Considering this, polymeric compounds made from PVDF and PMMA with different concentrations and solvents are fully described in this work. The novelty stands on efficiently process of polymer blend fabrication, by considering the learned issues. These are highlighted in the paper, concerning optical microscopy, and digital holographic microscopy. Films were made to carry out energy harvesting studies leading to knowing in detail its properties and characteristics, with emphasis in flexibility, homogeneity, and mechanical resistance. To do this, we obtain 2 and 3D surface images and analyze the electrical properties of the PVDF and PMMA mixtures. Next, the development of flexible translucent films of PVDF/PMMA hybrids formed with an approximate thickness of 100  $\mu\text{m}$  is presented, prepared by spin-coating technique with different weight percentage of PVDF in PMMA by means of a solution casting technique. The materials were characterized with Optical Microscope (OM), and Digital Holographic Microscope (DHM) techniques. Those characterizations confirmed that a concentration of 50 wt.% PMMA blend or higher makes the blend depart from granular to homogeneous aspect. Concentrations with a high percentage of PMMA show peaks and variation in surface uniformity using digital holography, which are represented as noticeable multicolored circles. A testing bench developed for

piezoelectric materials (EP2) served to estimate electrical performance.

## 2. EXPERIMENTAL SET UP

### 2.1. Polymer Films Preparation

Experimentally, 7 composites or blends are analyzed in which the amounts of PVDF and PMMA vary inversely proportional, from 0 to 100 wt.%. The selected percentages are shown in Table 1. For the blends, commercial PVDF and PMMA raw materials from Sigma-Aldrich were used, with  $M_w \sim 180,000$  and  $M_w \sim 120,000$ , respectively. The different amounts of PVDF and PMMA were dissolved in a mixture of two solvents: tetrahydrofuran (THF) (99.9%, from Fermont) and 1-Methyl-2-pyrrolidinone (NMP) ( $M_w \sim 99.15$ , assay: 99.5, from Sigma-Aldrich) [1].

**Table 1: Concentration of PVDF/PMMA films [1]**

Sample	PVDF/PMMA wt.%	Film
PVDF	100/0	PS
85PVDF	85/15	M1
70PVDF	70/30	M2
50PVDF	50/50	M3
30PVDF	30/70	M4
15PVDF	15/85	M5
PMMA	0/100	M6

To properly measure the weights of the polymers during the preparation of the blends, a *Sartorius*<sup>TM</sup> model CP324S precision analytical balance with a draft shield was used. It is worth mentioning that stirring bars were used in all samples to facilitate the dissolution of the polymers. The solvents were prepared in a 50/50 ratio (NMP/THF).

To make all the films, final composites were prepared with a concentration of 125mg/ml. Once the weight concentration was defined, the quantities of polymers (PVDF and PMMA and solvents (NMP/THF) corresponding to each sample were defined. It was decided to weigh 375mg of polymers in proportions for each sample and 3ml of solvent (NMP/THF 50/50).

The presentation of PVDF is in large grains, these were selected to approach the appropriate weight. However, when this was not achieved, appropriate adjustments were made to the PMMA and solvents. The calculated and real data for sample preparation are shown in Table 2.

**Table 2: Calculated and Real Data for Sample Preparation (PVDF/PMMA at 125mg/ml)**

Sample	Ideal Content						Real Content			
	PVDF/PMMA (%)		PVDF/PMMA (mg)		NMP/THF (ml)		PVDF/PMMA (mg)		NMP/THF (ml)	
PVDF	100	0	375	0	1.5	1.5	382	0	1.528	1.528
85PVDF	85	15	318.8	56.25	1.5	1.5	353.5	62.38	1.663	1.663
70PVDF	70	30	262.5	112.5	1.5	1.5	252.9	108.39	1.445	1.445
50PVDF	50	50	187.5	187.5	1.5	1.5	181.9	181.9	1.4552	1.4552
30PVDF	30	70	112.5	262.5	1.5	1.5	115.9	270.43	1.545	1.545
15PVDF	15	85	56.3	318.75	1.5	1.5	60.6	343.4	1.616	1.616
PMMA	0	100	0	375	1.5	1.5	0	364.5	1.458	1.458

The procedure to make each blend required 60 min of stirring at room temperature in an ultrasonic bath (Bransonic, Branson 2510R-DHT model), sufficient time to achieve complete dissolution of the polymers and adequate viscosity. After stirring, the polymer blends were deposited on Corning glass slides by spin coating at 5000 rpm. The resulting PVDF/PMMA films were subsequently dried in a vacuum oven under conditions of 50 kPa and 53°C. The drying process required remaining in the oven overnight to ensure the removal of solvent traces. Finally,  $\pm$ poled films were obtained by means of a layered deposit of silver paint on both sides of the film. After preparation, measurements were made.

## 2.2. Films Formation on Substrates

One of the techniques to obtain homogeneous and good quality thin films on flat substrates is the so-called spin-coating. In the process, an amount of solution is deposited on the substrate and the substrate is rotated at high speed to uniformly distribute this layer by centrifugal force. The rotation continues until the fluid travels to the edges of the substrate and until the desired layer thickness is achieved. The solvent used in the technique is volatile and evaporates, leaving the layer of material on the substrate, whose thickness depends on the rotation speed, the deposited material, and the solvent.

The film formation process consists of the following steps:

1. Cut and wash Corning glass substrates.
2. Configure the parameters on the equipment before starting sample preparation.
3. Place the Corning glass in the Spin-Coater
4. Take the required volume of the composite in solution (100  $\mu$ l) with the micropipette and deposit it on the Corning glass.
5. The nitrogen valve opens until 4 bars (approx. 60 psi) is reached.
6. The vacuum pump is turned on.
7. Start the spin-coating process.
8. The films are dried by evaporation of the solvent (NMP and THF).
9. At the end of the time, the vacuum pump is turned off and the nitrogen valve is closed.
10. Carefully remove the Corning glass with the deposited films, identify them and store them in sample holders (petri box) for later characterization.
11. Vary the parameters to achieve a film that completely covers the glass.
12. It is important that at the end of all the films the inside of the Spin-Coater is cleaned using a cotton with acetone.

Fabricating film on substrates requires combining operating parameters, including deposition time and spin speed, to achieve satisfactory results. After several failed tests, the required polymer film was obtained with the following parameters:

- Sample volume: 100 $\mu$ l.
- 5000 rpm.
- 2 min.
- 1 cycle.
- Nitrogen pressure of 4 bar.

So far films are ready to be studied, except for FTIR and the test bench. In this case the samples must be removed from the substrate and placed directly on the equipment. For the baking solidification process, a vacuum oven, Lab-Line™ and model 3608-5, and a vacuum pump, Vacuubrand® and model RZ 5, were used. Another option for solidification is grill, a StableTemp™ brand shaking rack was used. For both characterization methods, once the samples are dry, removed them from the substrate carefully, scraping one side and ending removing it with the help of tweezers. Two samples dried with different methods, with the same percentage of polymers (50PVDF), were analyzed by FTIR to see which drying method was better. The results are shown in Figure 1, similar spectra were obtained by both methods. However, vacuum drying is chosen instead of grilling because with this method the probability of sample contamination is lower.

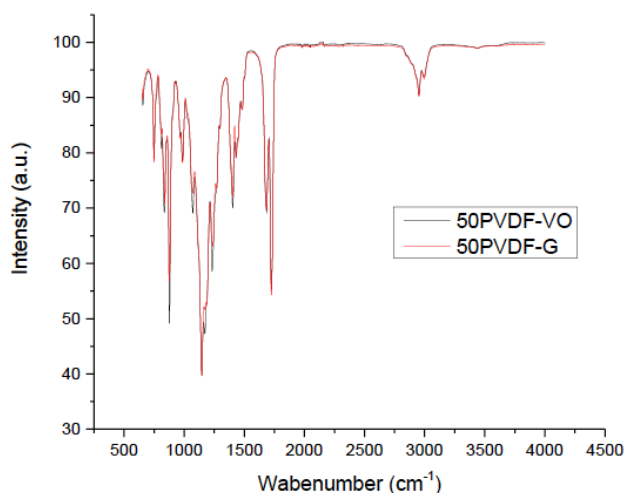


**Figure 1:** FTIR test used to choose a solidification method: 50PVDF-VO, sample in vacuum oven; 50PVDF-G, sample in grill.

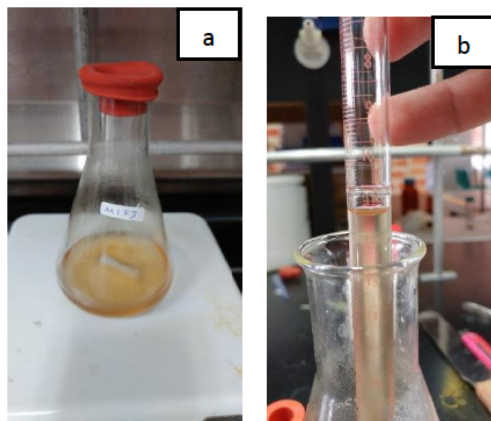


**Figure 2:** Solidification of samples. a) Sample under magnetic stirring. b) Taking out 20ml of sample with a pipette. c) Sample deposited in the Petri dish.

#### 2.1.4. Samples Preparation for Test Bench

The solidification of materials requires well-dissolved samples, for which an ultrasonic bath may be needed. The procedure begins with washing and drying the Petri dishes (5.2 c m in diameter) that will contain the samples. Using a pipette, doses of 10 or 20 ml of sample dissolved and stirring are taken. The samples remain inside the extraction hood until the solvent has evaporated. Afterwards, the samples are placed in the vacuum oven at an average temperature of 56 °C and left until the next day. Figures 2a-c describe these steps through images.

The product obtained is a thin film, which must be separated from the container carefully with a spatula to avoid breakage, see Figure 3.



**Figure 3:** Careful film separation.

#### 2.1.5. Film Thickness Measurement and Surface Treatment

While the film size is defined by the application, in present case the test bench requires a size 20x10 mm, which will be described later. A 10x10 mm test section is coated with liquid silver paint on both sides,

subsequently, a reduced area of 5x5 mm is coated on each side to make the sample conductive, leaving one corner free of coating. What this last step looks like is shown with a photograph in Figure 4, note that one corner is free of coating. Finally, the film is laminated by applying a thermo-mica, which must be sealed with an extra 5 mm all around.

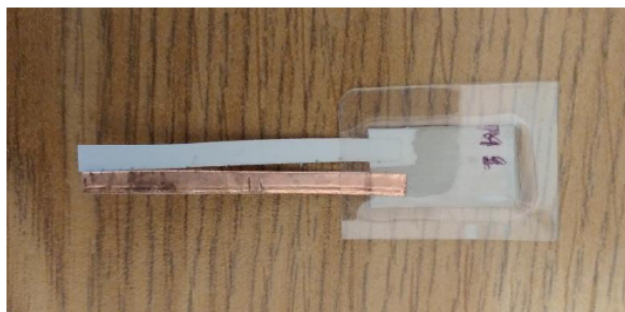


**Figure 4:** Painting and laminating of one film.

After cutting, painting, and laminating, two films were obtained for each sample. Note that when the PMMA content increased it produced an increase in thickness that varies from 1.03  $\mu\text{m}$  for the lowest content to 6.92  $\mu\text{m}$  for the maximum [1].

## 2.2. Microscopy Analysis

Film analysis by microscopy allows the detection of phase differences in materials. Changes can be detected by extremely small variations at the microstructure level. These are observed as intensity differences in the observed image, thus revealing features invisible under normal lighting. Electronic microscopy allows us to know the existence of several properties and characteristics, such as the  $\beta$ -phase, a compound property responsible for the voltage generation under strength-deformation.

### 2.2.1. Optical Microscope (OM)

To obtain OM digital images, a digital camera is installed. While the minimum and maximum magnification obtained with an Olympus model GX71 optical microscope are 50x and 2000x, the processing requires adaptation to data acquisition system. The main limitation is the wavelength of visible light, which limits the resolution of fine details in the solid sample. Also, an image capture application program is installed as a part of the equipment. This is a PixeLINK program, which eases the interpretation of images. Post processing includes retouching and editing with Photoshop Cs6 program, which converges the data from graphic to pixel format by Adobe Systems Inc.

### 2.2.2. Digital Holographic Microscope (DHM)

The construction of 3D images for one specific section of the surface of the samples is possible by implementing Digital Holographic Microscopy (DHM), called holographic interferometry too. DHM is a somewhat partially coherent source that detects phase displacement, improving the quality of the images. Implementation takes only a small fraction of the equipment cost, and it is applicable for superficial reconstruction of a sample. By reconstructing the interference phase, the tilt and curvature introduced by the optical system is removed. This allows us to observe the topography of the surface of the sample in a more precise and reliable way. As an example, holographic interferometry is used to compare 2 states, considering the first of them, a hologram of the reference wavefront of the holographic system (Figure 5a), and the second, a hologram directly from the object to be reconstructed (Figure 5b). Finally, to remove details from the hologram such as the inclination and curvature of the optical system the interference phase is determined (Figure 5c).

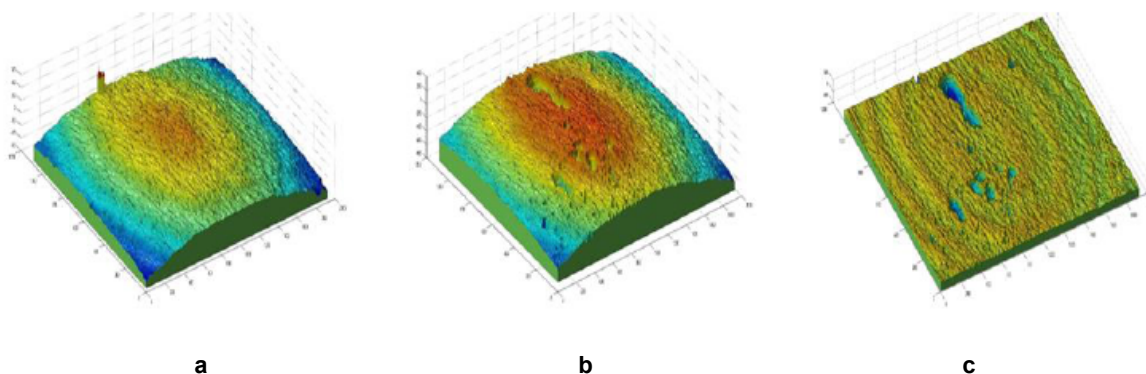


**Figure 5:** Comparison of states by holographic interferometry; a) Hologram of the reference wavefront; b) Hologram directly from the object; c) Interference phase is determined.

This method may be applicable at the laboratory level, even to develop it as a manufactured product, and a detailed description can be found elsewhere [30].

### 2.3. Test Bench for Piezoelectricity

The use of piezoelectric materials in their double function as sensors and transducers depends mostly on their location, the way in which they are subjected to excitation, and their topology-geometry. A test bench (EP1) reproduces the strength conditions in road applications such as tire belt to excite piezoelectric-type materials [30-31]. EP1 allows tests to be carried out where the speed of the wheels that excite the material as well as strength transmitted to it is adjustable. The bench was based on data reported elsewhere [30]. Piezoelectricity is evaluated by strength the PVDF/PMMA to produce a stress  $\sigma$ , which directly affects the charge generated, according to the expression:

$$C = \sigma \cdot d \cdot A \quad (1)$$

Where  $C$  represents the electric charge in Coulomb/second,  $\sigma$ ,  $d$ , and  $A$  mean the stress in pascals, the piezoelectric coefficient in Coulomb/Newton, and the surface area of the piezoelectric film exposed to strength in square meters, respectively [31].

The electric charge depends on the piezoelectric coefficient, which is a function of piezoelectric film thickness. This and other data are provided by the material manufacturer. Typical film aspects like 28  $\mu\text{m}$  thickness and its coefficient between  $d = 6 \times 10^{-12}$ , and  $10 \times 10^{-12}$  C/N are considered. The surface area to be deformed is 0.002  $\text{m}^2$ . The film is excited with

adjustable frequency to analyze its response through data reading equipment, a multi-meter, and a digital oscilloscope by Tektronix model TBS1102, see Figure 6a-c.

Another set-up different to EP1, the EP2, incorporates blades instead of rims to excite the films [31]. It also simulates the excitation conditions received by piezoelectric-type materials in road applications. A three-bladed variable speed turbine was mounted on the rotor shaft of a DC electric motor, see Figures 7a-b. As the turbine rotates on its axis, blade tips interact with the piezoelectric sample materials to produce a stress/strain detected as a voltage. The voltage is converted into an electrical current signal in a circuit built internally, see Figures 7c-d. The signal is displayed on a TBS1102 oscilloscope by Tektronix Inc., shown in Figure 7e. The signal is sent digitally to the computer for further analysis.

## 3. RESULTS AND DISCUSSION

This section first evaluates the results on chemical and physical stability of blend PVDF/PMMA, then it analyzes aspects as a source of power in tires, supported by tests conducted with benches EP1 and EP2. The results for films preparation are presented before discussing piezoelectricity.

### 3.1. Granular Morphology Detected by OM

The primary constraint of optical microscopy (OM) lies in the wavelength of visible light, a factor that directly influences the resolution of minute details within a solid sample. The limitations arise from the inherent properties of light, making it challenging to discern fine features at a microstructural level. The

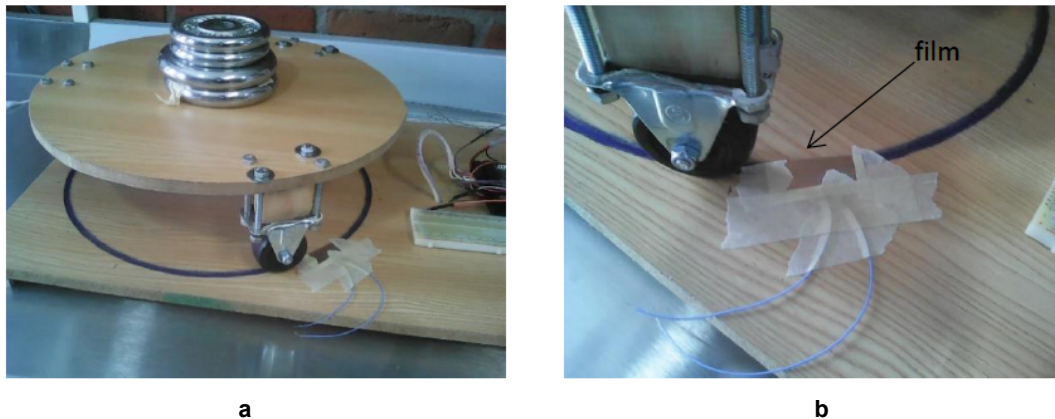


**Figure 6:** A first test bench used to evaluate piezoelectricity under road conditions, EP1; a) Test bench prototype to characterize piezoelectric materials by weight to adjust stress; b) Piezoelectric film attached to the base of the track of the rim of the test bench.

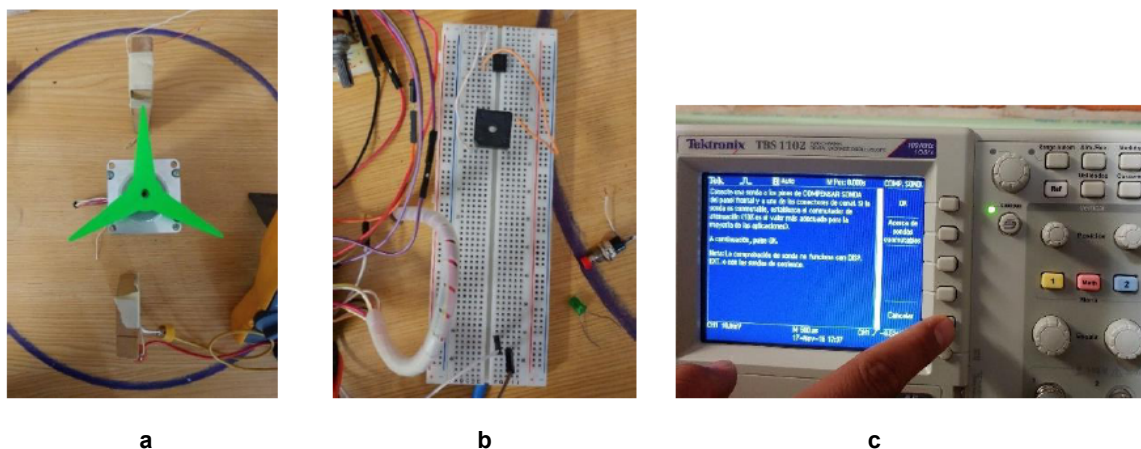


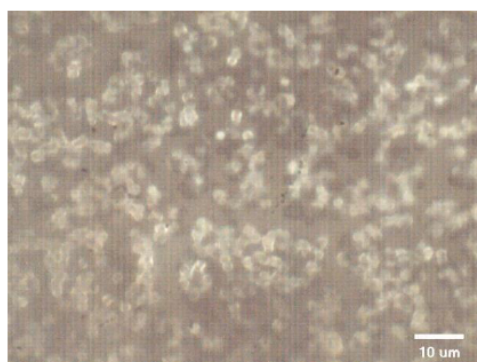
**Figure 7:** EP2 test bench used to evaluate piezoelectricity under road conditions; a) Turbine and electric motor in plan-view; b) Sample running test with circuit board; c) Visualization and analysis of analog signal processing.

phase variations induced by minuscule irregularities within the microstructure are subsequently translated into discernible intensity differences in the observed image. This transformative process unveils characteristics that remain unseen under conventional lighting conditions. Figure 8 present a visual representation showcasing images captured through OM, specifically highlighting different concentrations of PVDF/PMMA. Through the lens of optical microscopy, these images not only capture the structural nuances of the material but also bring to light subtle variations in concentration. This serves as a testament to the power of OM in revealing hidden details and providing valuable insights into the composition and characteristics of the studied samples.

Figures 8a-6f highlight that PMMA has a much smoother morphology than PVDF. The PVDF shows a granular morphology, which changes with the concentration of the polymers in the blend: As the PMMA phase increases, the granular morphology of the PVDF decreases. In PMMA/PVDF composites, by increasing the concentration of PVDF in PMMA, the morphology of the blend is more like that of pure

PVDF. It can be said that from a PVDF concentration of 85% the morphology is almost the same to that of pure PVDF. The PVDF crystals are hidden as the PMMA concentration increases, that is, the greater the presence of PMMA, the lesser the PVDF crystals. In the images of the samples PVDF, Figure 8a, and PMMA, Figure 8g, both polymers are clearly visible, the PVDF in the form of crystals and the PMMA with smooth morphology. In the images of the samples 85PVDF, 70PVDF and 50PVDF, Figure 8b to Figure 8d, small sections of these polymers are grouped. However, in sample 30PVDF, the image of Figure 8e shows how the PVDF granules are no longer visible because they have completely covered by the PMMA. In the following figures, 15PVDF and PMMA Figure 8f and Figure 8g respectively, the shapes are lost and give rise to a practically uniform mix.

Figures 8a-6f illuminate a stark contrast in morphology between PMMA and PVDF, revealing distinctive characteristics in their structural compositions. Notably, PMMA exhibits a markedly smoother morphology in comparison to the granular structure observed in PVDF. The granular morphology



a



b

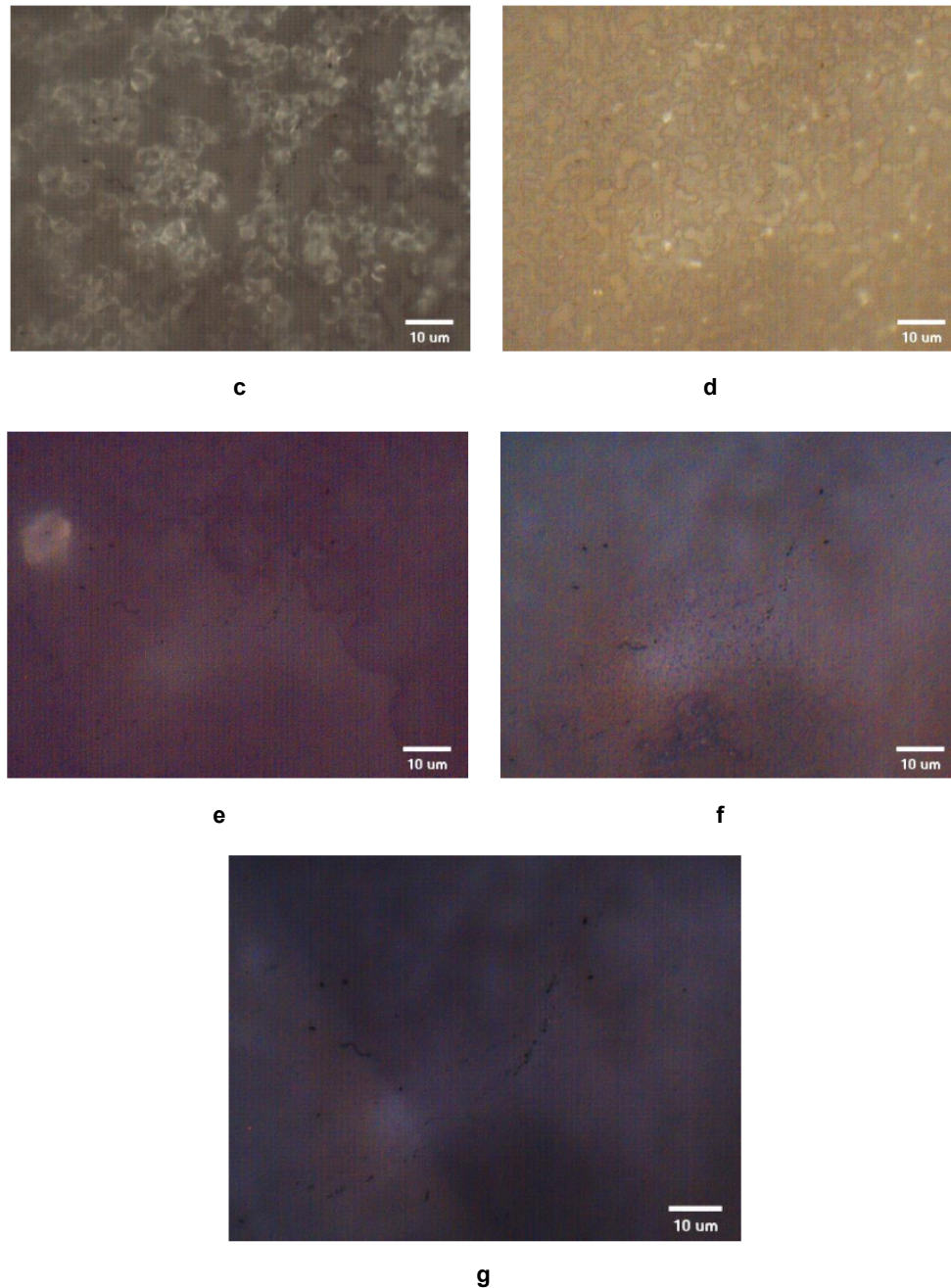


**Figure 8:** Morphology of several PVDF/PMMA samples through the optical microscope; **a)** Pure PVDF; **b)** 85PVDF; **c)** 70PVDF; **d)** 50PVDF; **e)** 30PVDF; **f)** 15PVDF; **g)** Pure PMMA.

of PVDF, intriguingly, undergoes alterations in response to variations in polymer concentration within the blend. As the proportion of the PMMA phase increases, there is a discernible reduction in the granular features of PVDF.

Within the PMMA/PVDF composites, manipulating the concentration of PVDF in PMMA leads to a morphological shift towards a resemblance to pure PVDF. It becomes apparent that beyond a PVDF concentration of 85%, the morphology closely mirrors that of pure PVDF. Interestingly, the presence of PVDF

crystals becomes increasingly obscured with rising PMMA concentration; in essence, a higher prevalence of PMMA correlates with a diminished presence of PVDF crystals.

Examining specific samples, such as PVDF (Figure 8a) and PMMA (Figure 8g), vividly showcases the distinct characteristics of each polymer. PVDF manifests in crystal form, while PMMA exhibits a notably smooth morphology. Samples like 85PVDF, 70PVDF, and 50PVDF (Figure 8b to Figure 8d) reveal consolidated sections of these polymers, offering

insights into the evolving blend morphology. However, in the case of sample 30PVDF, as depicted in Figure 8e, the granular features of PVDF are entirely obscured, now concealed by the encompassing PMMA.

Moving forward to samples 15PVDF and PMMA (Figure 8f and Figure 8g), a noteworthy transformation unfolds, as the distinct shapes gradually dissipate, giving rise to a nearly uniform amalgamation. This visual evolution underscores the dynamic interplay between PVDF and PMMA concentrations, shaping the overall morphology of the composite blend into a homogenous and integrated form.

### 3.2. Colored Structure Using DHM

The Digital Holographic Microscopy (DHM) method presents a transformative approach, enabling the examination of an entire sample with unparalleled efficiency. Unlike the conventional optical microscope, where fields of vision are circular, DHM utilizes rectangular fields of vision, allowing for the comprehensive analysis of 100% of a sample. This departure from circular fields not only maximizes the observational scope but also contributes to a more exhaustive understanding of the sample's characteristics.

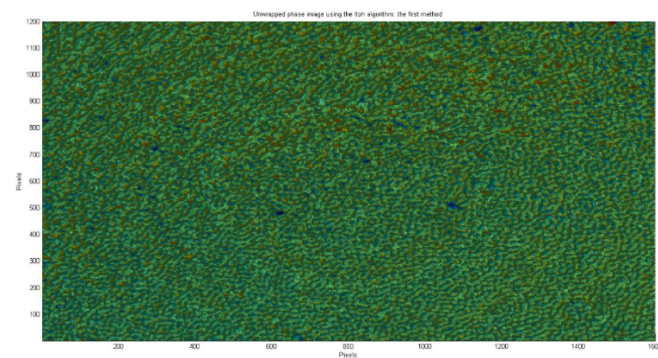
One notable advantage of DHM lies in its elimination of the demanding focusing process. Unlike traditional methods, DHM provides information for various distances ( $d$ ), obviating the need for meticulous and strenuous manual focusing. This streamlined approach enhances the speed and accuracy of sample analysis, making it a valuable tool for researchers and practitioners alike.

The ensuing results, sequentially presented from Figure 9a onward, encapsulate the profound insights gained through DHM. Figure 9a serves as a visual representation of the pure PVDF surface, where the uniformity of color under the influence of light is evident. Moving to Figures 9b-d, the subsequent images depict samples corresponding to blends 85PVDF, 70PVDF, and 50PVDF. These figures unveil a nuanced morphology, deviating slightly from that of pure PVDF, marked by subtle variations in colored structures.

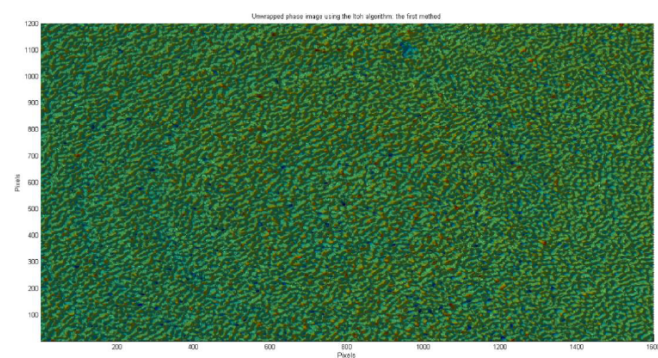
It is essential to underscore the intricacies of DHM, wherein two unwrapped images in phase play a pivotal role—one serving as a reference and the other corresponding to the sample under investigation. When

capturing images, the inherent curvature introduced by microscope lenses and objectives poses a challenge. This curvature is systematically addressed by subtracting it, resulting in the acquisition of a flat image that facilitates a more accurate analysis.

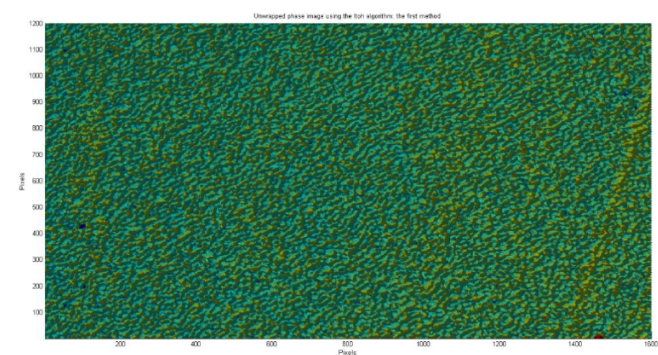
In the context of the sample, it is imperative to recognize that complete light penetration does not occur uniformly. This disparity is contingent upon various factors, such as the concentration of the material. Higher concentrations exhibit increased light absorption, introducing a variable that significantly influences the obtained results. The thickness of layers and the opacity of samples emerge as critical considerations, wielding a substantial impact on the overall outcomes.



a



b



c

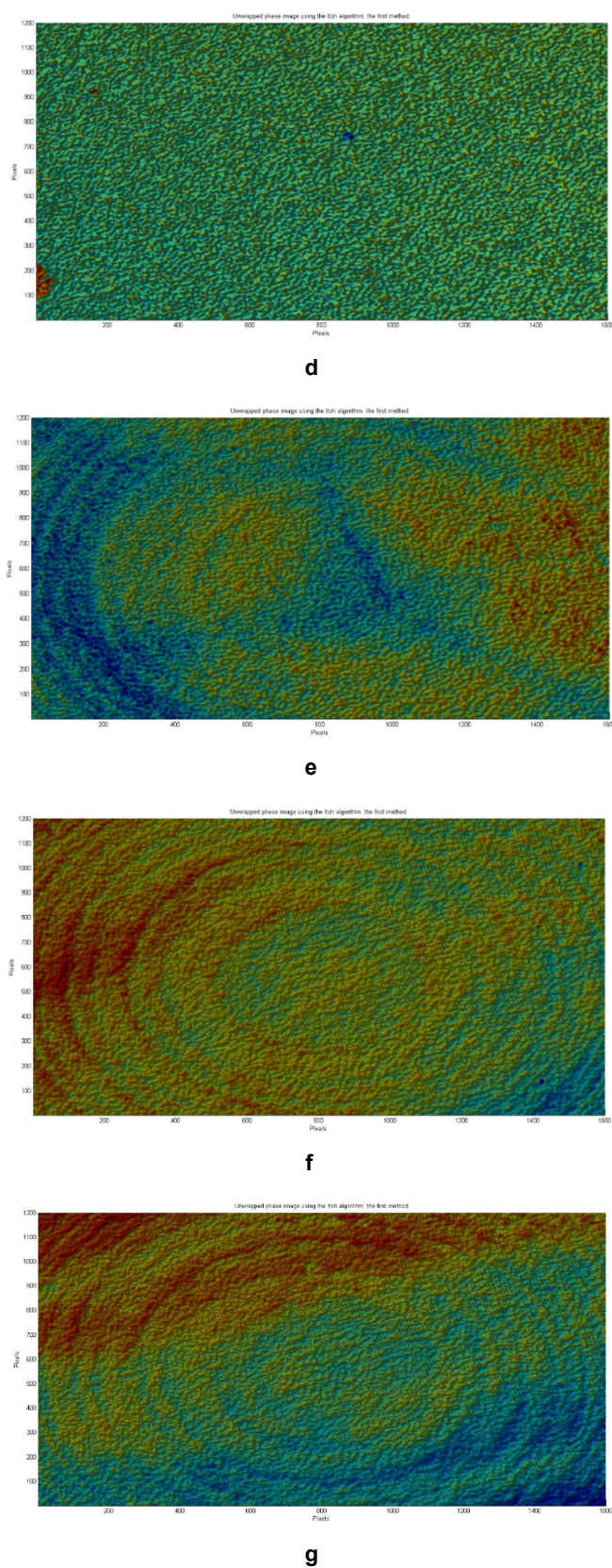


**Figure 9:** Colored structure of several PVDF/PMMA samples through the optical microscope, scale (1600,1200) in pixels (x,y); **a)** Pure PVDF; **b)** 85PVDF; **c)** 70PVDF; **d)** 50PVDF; **e)** 30PVDF; **f)** 15PVDF; **g)** Pure PMMA.

The diverse spectrum of colors observed in DHM results is intricately linked to the morphology of the sample. Notably, the height of peaks in the sample's morphology dictates the variation in colors—red signifies peaks with considerable height, while blue corresponds to valleys situated at the bottom. Consequently, red hues indicate areas where a reduced amount of light has traversed the sample.

Examining Figures **9e** to **9g**, which portray outcomes for samples characterized by the highest PMMA content (ranging from 30PVDF to pure PMMA), a visually captivating display unfolds. The intricate morphology elicits the appearance of red hues with accompanying blue traces and intermittent yellow tones, intricately distributed across distinct zones. Figure **9d**, corresponding to the sample with 70% PMMA, exhibits a subtle red tone. However, as the concentration of PMMA escalates (as evident in Figures **9e** and **9f**), the prevalence of the red phase intensifies. Notably, in samples 30PVDF and 15PVDF, the morphology begins to mirror that of PMMA, as illustrated in Figure **9g**. Meanwhile, the remaining compounds (50PVDF, 70PVDF, and 85PVDF) exhibit morphologies more closely aligned with that of pure PVDF.

This expanded version provides a more detailed exploration of the complexities involved in DHM, shedding light on the considerations and variables that shape the observed results.

### 3.3. Piezoelectric Performance

The influence of PVDF concentration on film properties is meticulously examined through the analysis of registered data, specifically measuring voltage from EP2. This multifaceted evaluation extends to the frequency domain, where the film undergoes strength testing induced by the rotational movement of a turbine at a frequency of 200 Hz. The analogical response is meticulously recorded and subsequently digitalized, presenting a wealth of insights into the piezoelectric characteristics of the films.

Table **3** encapsulates the comprehensive results derived from each sample, delineating the maximum and minimum values of voltage in the initial columns. A discernible trend emerges, underscoring the pronounced impact of PVDF concentration on the piezoelectric response. Notably, the voltage peaks with the highest amplitude are evident for both the commercial and pure PVDF polymer. However, a

**Table 3: Piezoelectricity Effect of Several Samples of PVDF/PMMA**

Film	Voltage (V)		Frequency (Hz)		Current @5 V [2] (pA)
	Max	Min	Max	Min	
SP	0.632	0.33	235.3	175.1	
PVDF	0.29	0.175	60.02	41.62	6.9
85PVDF	0.171	0.096	38.79	8.77	13.5
70PVDF	0.1	0.053	1.72	0	95.5
50PVDF	0.141	0.062	2.16	8.44	45.1
30PVDF	0.115	0.058	2.41	1.98	7.8
15PVDF	0.117	0.07	1.94	1.45	5.0
PMMA	0.102	0.02	1.77	1.45	5.4

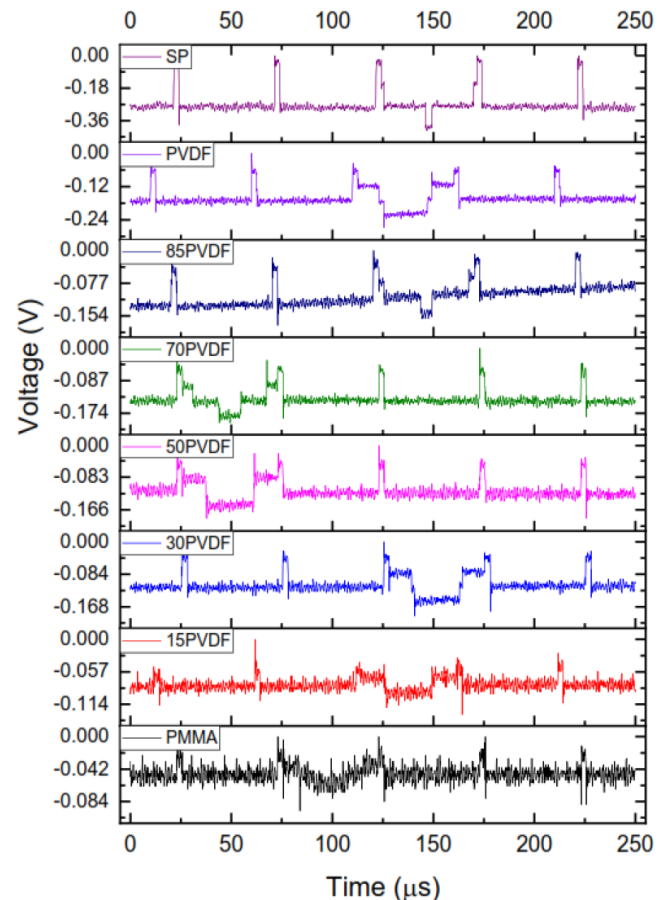
noteworthy decline in voltage is observed as the PVDF content diminishes. The stability of the pure PVDF film is brought into question, particularly as its minimal voltage registers as null. Intriguingly, the commercial film SP exhibits the smallest gap between maximum and minimum voltage, raising interesting considerations about its performance.

Delving into the electric current aspect, column five of Table 3 delineates the recorded values. A 5 V voltage application serves as the excitation stimulus for the films, with the film sample containing 70 wt% PVDF demonstrating the maximum response, consistent with findings reported elsewhere [2]. It is noteworthy that results obtained with a 10 V excitation voltage (not explicitly shown) exhibit values that are twice those detailed in column five, further emphasizing the correlation between excitation voltage and the piezoelectric response of the films. These nuanced insights into the electrical characteristics of the films deepen our understanding of the intricate interplay between PVDF concentration and the resulting piezoelectric behavior.

The recorded frequency data exhibits a noticeable decline, ranging from the maximum value documented for the commercial SP film to 1.45 Hz for the pure PMMA film. This frequency variation is attributed to the active PVDF material, wherein the presence of higher concentrations facilitates the oscilloscope's ability to detect signals more effectively. The observed shift in frequency holds significant implications, particularly in the realm of energy harvesting device design, where the frequency of voltage generation plays a pivotal role.

In Figure 10, temporal voltage signals for each film (refer to Figure 1) are depicted, sourced from the recorded data observed on the oscilloscope. Evidently,

voltage peaks exhibit high frequencies for the PS film, as illustrated in the voltage-versus-time plot showcased in Figure 10. Notably, these voltage peaks become less frequent with an increase in PMMA concentration. The averaged and maximum voltage values are employed to present a comprehensive overview of the results for each film, spanning from SP to PMMA, in the plot illustrated in Figure 11.

**Figure 10:** Voltage signal from bench EP2 for several samples, where SP means commercial films.

The voltage trend across the films demonstrates a decay from the maximum observed for the commercial SP film as the PVDF content decreases, eventually reaching the film sample 70PVDF. An intriguing inflection point is observed for the film sample 50PVDF, indicating a subtle recovery, a phenomenon evident in both maximum and averaged values. This nuanced change, observed particularly in the in-house developed samples, signifies the intricate interplay between PVDF content and the resulting voltage response.

Noteworthy is the comparison with PS, where the difference between maximum and averaged values is nearly twice as pronounced only for the commercial sample, not mirrored in the in-house developed samples. This minimal gap is indicative of a consistent response, underscoring the pivotal role played by PMMA content. PMMA's contribution in elevating the  $\beta$  phase in the composite is emphasized, elucidating its role in conferring the piezoelectric property, as discussed elsewhere [1-2].

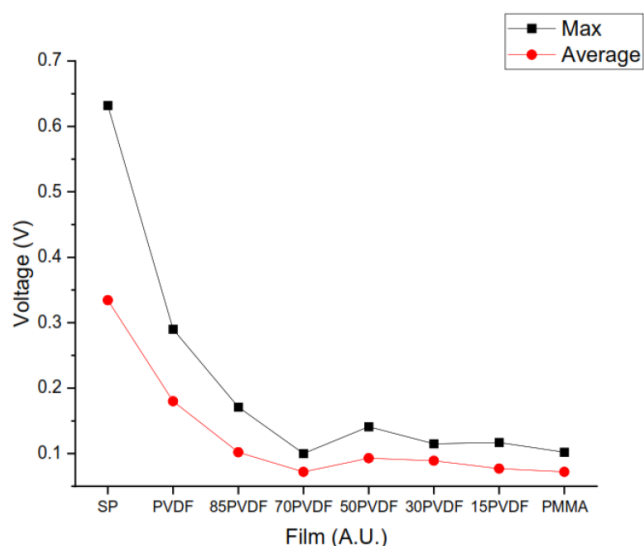


**Figure 11:** Mark sensor and samples (PVDF/PMMA) voltages in test bench; SP: commercial film; PVDF: pure PVDF; 85PVDF: 85/15; 70PVDF: 70/30; 50PVDF: 50/50; 30PVDF: 30/70; 15PVDF: 15/85 and PMMA: pure PMMA.

#### 4. CONCLUSIONS

This work has addressed the methodology adopted for developing and evaluating piezoelectric polymeric materials, focusing on the behavior of PVDF/PMMA in different concentrations. Optically, the sample films developed are discussed through images with broad strokes of polymer variations, which are well defined in color by holographic plates. As the contents of PMMA

increases, the granular structure of PVDF decreases until a smooth morphology is achieved. The study reveals a high compatibility of PVDF with PMMA with advantages in their conductive properties. The methodology used allowed us to identify properties for a wide spectrum of concentration in the blends of polymers under analysis. It revealed that lamination and encapsulation of piezoelectric films have important effects, like small separation of the film particles at the time the rest of evaporated solvent. When laminating occurs, it was with very thick and low flexibility films. Film coating also affects voltage reading data applying controlled strength to produce the stress on the films even with precise instrumentation. The process of polymer blend fabrication may be more efficient if leaned issues are applied as highlighted in the paper, which were observed during optical microscopy, and digital holographic microscopy.

#### ACKNOWLEDGEMENTS

This work was supported by the National Council of Science and Technology CONACyT-Mexico with first author scholarship CB-2015/255512. Thanks are given to Higher Education Program PRODEP for the support through project 511/2022-5257-742. Thanks to Dr. R. Guardián for OM images, to Dr. Darwin and V. Juárez for sharing a hand on DHM, and to A. Beltrán for lending and guiding on the use of device EP2.

#### AVAILABILITY OF DATA AND MATERIAL

The datasets generated during and/or analyzed during the current study are available from the corresponding author on reasonable request.

#### FINANCIAL INTERESTS

The authors declare they have no financial interests.

#### AUTHOR CONTRIBUTION STATEMENT

All authors contributed to material preparation, data collection and analysis. Conception and investigation were performed by [J.R. Leppe-Nerey, F.Z. Sierra-Espinosa, and M.E. Nicho]. The first draft of the manuscript was written by [J.R. Leppe-Nerey, F.Z. Sierra-Espinosa, and M.E. Nicho] and authors [M.A. Basurto and J.A. Rodríguez] contributed with signal processing and mechanical properties, respectively. All authors read and approved the final manuscript.

## FUNDING STATEMENT

This study was funded by [National Council of Science and Technology CONACyT-Mexico with first author postdoctoral grant CB-2015/255512]. The Mexican Program for Higher Education, PRODEP supported with Academic Body project 511/2022-5257-742.

## REFERENCES

- [1] Leppe-Nerey JR, Nicho ME, Sierra-Espinosa FZ, Hernández-Guzmán F, Fuentes-Pérez M (2021) Experimental study of piezoelectric polymeric film as energy harvester. *Materials Science and Engineering: B* 272: 115366. <https://doi.org/10.1016/j.mseb.2021.115366>
- [2] Leppe-Nerey JR, Sierra-Espinosa FZ, Nicho ME, Basurto-Pensado MA (2021) Power characteristics of a 70/30 wt.% PVDF/PMMA film in roadway electricity generation. *Sens Actuators A Phys* 317: 112461. <https://doi.org/10.1016/j.sna.2020.112461>
- [3] Pike E (2011) Oportunidades de uso eficiente de los neumáticos
- [4] Kang G Dong, Cao Y ming (2014) Application and modification of poly(vinylidene fluoride) (PVDF) membranes - A review. *J Memb Sci* 463: 145-165. <https://doi.org/10.1016/j.memsci.2014.03.055>
- [5] Jeedi VR, Narsaiah EL, Yalla M, Swarnalatha R, Reddy SN, Sadananda Chary A (2020) Structural and electrical studies of PMMA and PVdF based blend polymer electrolyte. *SN Appl Sci* 2: 2093. <https://doi.org/10.1007/s42452-020-03868-8>
- [6] Kawai H (1969) The Piezoelectricity of Poly (vinylidene Fluoride). *Jpn J Appl Phys* 8: 975-976. <https://doi.org/10.1143/JJAP.8.975>
- [7] Choi S, Jiang Z (2006) A novel wearable sensor device with conductive fabric and PVDF film for monitoring cardiorespiratory signals. *Sens Actuators A Phys* 128: 317-326. <https://doi.org/10.1016/j.sna.2006.02.012>
- [8] Saunier J, Alloin F, Sanchez JY, Barrière B (2004) Plasticized Microporous Poly(vinylidene fluoride) Separators for Lithium-Ion Batteries. I. Swelling Behavior of Dense Membranes with Respect to a Liquid Electrolyte - Characterization of the Swelling Equilibrium. *J Polym Sci B Polym Phys* 42: 532-543. <https://doi.org/10.1002/polb.10730>
- [9] Kang SJ, Park YJ, Bae I, Kim KJ, Kim HC, Bauer S, Thomas EL, Park C (2009) Printable ferroelectric PVDF/PMMA blend films with ultralow roughness for low voltage non-volatile polymer memory. *Adv Funct Mater* 19: 2812-2818. <https://doi.org/10.1002/adfm.200900589>
- [10] Deeba F, Gupta AK, Kulshrestha V, Bafna M, Jain A (2022) Investigations on dielectric properties of PVDF/PMMA blends. *Mater Today Proc* 66: 3547-3552. <https://doi.org/10.1016/j.matpr.2022.06.417>
- [11] Laroche G, Lafrance CP, Prud'homme RE, Guidoin R (1998) Identification and quantification of the crystalline structures of poly(vinylidene fluoride) sutures by wide-angle X-ray scattering and differential scanning calorimetry. *J Biomed Mater Res* 39: 184-189. [https://doi.org/10.1002/\(SICI\)1097-4636\(199802\)39:2<184::AID-JBM3>3.0.CO;2-L](https://doi.org/10.1002/(SICI)1097-4636(199802)39:2<184::AID-JBM3>3.0.CO;2-L)
- [12] Charlot B, Gauthier S, Garraud A, Combette P, Giani A (2011) PVDF/PMMA blend pyroelectric thin films. *Journal of Materials Science: Materials in Electronics* 22: 1766-1771. <https://doi.org/10.1007/s10854-011-0360-7>
- [13] Shah D, Maiti P, Gunn E, Schmidt DF, Jiang DD, Batt CA, Giannelis EP (2004) Dramatic enhancements in toughness of polyvinylidene fluoride nanocomposites via nanoclay-directed crystal structure and morphology. *Advanced Materials* 16: 1173-1177. <https://doi.org/10.1002/adma.200306355>
- [14] Park YJ, Kang YS, Park C (2005) Micropatterning of semicrystalline poly(vinylidene fluoride) (PVDF) solutions. *Eur Polym J* 41: 1002-1012. <https://doi.org/10.1016/j.eurpolymj.2004.11.022>
- [15] Sun J, Yao L, Zhao Q-L, Huang J, Song R, Ma Z, He L-H, Huang W, Hao Y-M (2011) Modification on crystallization of poly(vinylidene fluoride) (PVDF) by solvent extraction of poly(methyl methacrylate) (PMMA) in PVDF/PMMA blends. *Front Mater Sci* 5: 388-400. <https://doi.org/10.1007/s11706-011-0152-2>
- [16] Hirata Y, Kotaka T (1981) Phase separation and viscoelastic behavior of semicompatible polymer blends: Poly(vinylidene fluoride)/poly(methyl methacrylate) system. *Polym J* 13: 273-281. <https://doi.org/10.1295/polymj.13.273>
- [17] Elashmawi IS, Hakeem NA (2008) Effect of PMMA addition on characterization and morphology of PVDF. *Polym Eng Sci* 48: 895-901. <https://doi.org/10.1002/pen.21032>
- [18] Gregorio RJr, NCP de Souza N (1995) Effect of PMMA addition on the solution crystallization of the  $\alpha$  and  $\beta$  phases of poly(vinylidene fluoride) (PVDF). *J Phys D Appl Phys* 28: 432-436. <https://doi.org/10.1088/0022-3727/28/2/028>
- [19] Wankhade SH, Tiwari S, Gaur A, Maiti P (2020) PVDF-PZT nanohybrid based nanogenerator for energy harvesting applications. *Energy Reports* 6: 358-364. <https://doi.org/10.1016/j.egy.2020.02.003>
- [20] Uddin ASMI, Lee D, Cho C, Kim B (2022) Impact of Multi-Walled CNT Incorporation on Dielectric Properties of PVDF-BaTiO<sub>3</sub> Nanocomposites and Their Energy Harvesting Possibilities. *Coatings* 12: 77. <https://doi.org/10.3390/coatings12010077>
- [21] Bodkhe S, Rajesh PSM, Kamle S, Verma V (2014) Beta-phase enhancement in polyvinylidene fluoride through filler addition: Comparing cellulose with carbon nanotubes and clay. *Journal of Polymer Research* 21: 434. <https://doi.org/10.1007/s10965-014-0434-3>
- [22] Wang SH, Wan Y, Sun B, Liu LZ, Xu W (2014) Mechanical and electrical properties of electrospun PVDF/MWCNT ultrafine fibers using rotating collector. *Nanoscale Res Lett* 9: 1-7. <https://doi.org/10.1186/1556-276X-9-522>
- [23] Gupta P, Rajput M, Singla N, Kumar V, Lahiri D (2016) Electric field and current assisted alignment of CNT inside polymer matrix and its effects on electrical and mechanical properties. *Polymer (Guildf)* 89: 119-127. <https://doi.org/10.1016/j.polymer.2016.02.025>
- [24] Wattanasarn H (2020) Step Synthesis, Electrical Generator of PVDF / CNTsPiezoelectric. *12*: 35-41.
- [25] Misiurev D, Țălu Ș, Dallaev R, Sobola D, Goncharova M (2021) Preparation of PVDF-CNT composite. *E3S Web of Conferences* 270: 1-8. <https://doi.org/10.1051/e3sconf/202127001012>
- [26] Yu S, Zheng W, Yu W, Zhang Y, Jiang Q, Zhao Z (2009) Formation mechanism of  $\beta$ -phase in PVDF/CNT composite prepared by the sonication method. *Macromolecules* 42: 8870-8874. <https://doi.org/10.1021/ma901765j>
- [27] Wang Y, Lei D, Wu L, Ma R, Ning H, Hu N, Lee A (2023) Effects of stretching on phase transformation of PVDF and its copolymers: A review, *Open Physics* 21: 20220255. <https://doi.org/10.1515/phys-2022-0255>

- [28] Cui Y, Sui Y, Wei P, Lv Y, Cong Ch, Meng X, Ye H-M, Zhou Q (2023) Rationalizing the Dependence of Poly (Vinylidene Difluoride) (PVDF) Rheological Performance on the Nano-Silica. *Nanomaterials* 13: 1096.  
<https://doi.org/10.3390/nano13061096>
- [29] Pawde SM, Deshmukh K (2009) Investigation of the structural, thermal, mechanical, and optical properties of poly(methyl methacrylate) and poly(vinylidene fluoride) blends. *J Appl Polym Sci* 114: 2169-2179.  
<https://doi.org/10.1002/app.30641>
- [30] Vázquez Rodríguez M, Jiménez Martínez FJ, De Frutos J (2011) Banco de ensayos para materiales piezoeléctricos en aplicaciones viales. *Boletín de la Sociedad Española de Cerámica y Vidrio* 50: 65-72.  
<https://doi.org/10.3989/cyv.092011>
- [31] Varela CA, Sierra FZ (2014) Cyclic strain rate in tyres as power source to augment automobile autonomy. *International Journal of Vehicle Design* 65: 270-285.  
<https://doi.org/10.1504/IJVD.2014.060806>

---

Received on 20-10-2023

Accepted on 24-11-2023

Published on 28-11-2023

DOI: <https://doi.org/10.31875/2410-2199.2023.10.07>

© 2023 Leppe-Nerey *et al.*; Zeal Press.

This is an open access article licensed under the terms of the Creative Commons Attribution License

(<http://creativecommons.org/licenses/by/4.0/>) which permits unrestricted use, distribution and reproduction in any medium, provided the work is properly cited.